




Review Paper

# The capability of Ansys CFX to predict the mixing phenomena in ROCOM test facility

M. Boumaza<sup>1</sup>  · T. Höhne<sup>2</sup> · B. Mohammedi<sup>1</sup> · R. Dizene<sup>3</sup>

Received: 26 June 2019 / Accepted: 25 October 2019 / Published online: 20 November 2019  
© Springer Nature Switzerland AG 2019

## Abstract

This work consists of a Computational Fluid Dynamics (CFD) modeling of a reference experiment on boron dilution in the Rossendorf coolant mixing Model (ROCOM) as part of a coordinated research project of the International Atomic Energy Agency, namely, “Application of numerical codes of fluid dynamics to the design of nuclear power plants”. This coordinated project aims to address the application of CFD codes to the process of optimizing the design of nuclear power plants related to pressurized water reactors and to evaluate the performance and predictive capabilities of these codes and to contribute to their validation. In this context, a three-dimensional numerical simulation study was carried out using CFD code ANSYS CFX v14.5, to study the boron mixing phenomenon at the core inlet and the downcomer of the ROCOM test facility. The phenomenon of experimental mixing occurs by the injection of a tracer (sodium chloride) into one of the loops of the ROCOM installation mainly containing demineralized water in its primary circuit. The concentration field of the tracer is measured and simulated at the entrance of the heart and in the lowering. The SST-kw turbulence model used in this study could reasonably predict the distribution of the injected tracer in measurement locations within the test facility. The results of this numerical simulation were compared to the Benchmark data provided by the ROCOM experimental facility of the Helmholtz-Zentrum Dresden-Rossendorf Institute.

**Keywords** Boron dilution · CFD codes · Mixing

## 1 Introduction

The numerical simulation of fluid dynamics through CFD codes has become a necessary step before any development or design of devices whose operation is related to the circulation of a fluid. The application of CFD codes in the field of nuclear safety will be considered once they are properly verified and validated, to replace some expensive experimental tests associated with the design of a nuclear power plant, because the use of such codes is likely to provide qualitative services and quantitative information in many key areas for which traditional design tools are limited especially when a three-dimensional fluid movement

is required in the physical problem. CFD (Computational Fluid Dynamics) is already well established in other important industrial fields, such as aerospace, automotive, chemistry and other fields [1].

Experimental validation of CFD codes through Benchmarks in the field of thermal-hydraulic is necessary. Over time, several techniques have been developed for this purpose. Among these, the laser technology currently used in the ROCOM test facility, this recent, innovative, promising technology is flexible enough to be adapted to a wide variety of flows. Thanks to this technique, the test time is considerably reduced. Besides this, there is the technique of special metal mesh sensors, based on the measurement

✉ M. Boumaza, m\_boumaza03@hotmail.fr | <sup>1</sup>Thermohydraulic Department, Nuclear Research Centre of Birine (CRNB), POBox 180, DZ 17200 Ain Oussera, Djelfa, Algeria. <sup>2</sup>CFD Department, Institute of Fluid Dynamics, Helmholtz-Zentrum Dresden-Rossendorf (HZDR), POBox 51 01 19, 01314 Dresden, Germany. <sup>3</sup>University of Science and Technology Houari Boumediene, Bab Ezzouar, Algeria.



of the electrical conductivity of the liquid for the measurement of salty tracer, which has been developed and adopted by the same facility [2].

This work is one of my CFD code simulation activities, Ansys CFX in this case, in the IAEA technical staff member assigned to lead Coordinated Research Project (CRP), titled: Application of Computational Fluid Dynamics CFD Codes for Nuclear Power Plant Design, code I31022. This project deals with the application of CFD codes to the process of optimizing the design of nuclear power plants for pressurized (water-cooled) water reactors. This coordinated project aims to evaluate the performance and predictive capability of CFD codes and to contribute to their verification and validation. The study of the distribution of the boron concentration at the inlet core following the injection of deborated water and its mixing is the main objective of this benchmark provided by ROCOM test facility for the validation of the various CFD codes used by participants in this coordination project. In this context, a three-dimensional numerical simulation study was carried out using the ANSYS CFX v14.5 CFD code to follow the transport of the injected tracer and its mixing with the demineralized water present in the cold legs and the downcomer of ROCOM test facility.

This composed study of simulation and experimental, also represents in the real case the boron dilution in the primary fluid, under certain accidental conditions in a pressurized water reactor primary circuit.

An accident of loss of primary coolant (LOCA) in a PWR reactor arises from a breach affecting its primary circuit, or a circuit connected to it. This type of accident can lead to a boron dilution in the primary circuit and consequently to a heterogeneous distribution of boron in the reactor pressure vessel. Next, to this, the boron dilution inside the primary circuit may refer to a transient situation, when the boron content in certain parts of the primary circuit fluid is lower than the nominal value, a water plug with a low boron concentration can form in the primary circuit by various mechanisms. The most obvious mechanisms are the injection of fluid with low boron content in the primary circuit from external injection systems such as the reactor chemical and volumetric control (RCV) or another physical mechanism as the separation of the cooling fluid by the condensation process in the steam generator during a breach on a pipe connected thereto. The conclusion that has been drawn from the literature search shows that the good mixing of coolant and boron injected into the primary circuit is of great interest for two classes of accident scenarios: boron dilution and transient injection of cold water [3]. For the study of this mixing phenomenon, the ROCOM test facility was designed by the Dresden-Rossendorf research center (FZD) on scaling of 1:5, simulating the German KONVOI reactor. The experimental measurements dedicated by

this test facility are two types: Measurement of the flow velocity at the downcomer by the high-performance LDA technique and measurement of the concentration of the tracer injected into the cold legs of the test facility using the (mesh-sensors) which are implanted and distributed in the upper and lower Downcomer as well as at the core inlet of the test facility. These electrical conductivity sensors can provide detailed information on the spatial.

## 2 Modeling of the transport equation of a passive scalar

The transport of a passive scalar by a turbulent flow is frequently encountered in many industrial applications. The difficulty in predicting the dynamics of a scalar comes mainly from the turbulent nature of the flow that carries it [4].

The transport equation of a passive scalar  $c$  without source term is written:

$$\frac{\partial C}{\partial t} - D \frac{\partial^2 C}{\partial x_j^2} + \bar{u}_j \frac{\partial C}{\partial x_j} = 0 \quad (1)$$

where  $D$  ( $m^2 s^{-1}$ ) is the diffusivity of the passive scalar in the fluid and  $\bar{u}_j$  the mean velocity of the flow.

In this case study, the fluid is supposed to be incompressible; the scalar field is represented in space and time by  $C(x, t)$ . If we apply the Reynolds decomposition on the advection–diffusion Eq. (1) which governs the evolution of a passive scalar field, and in mean, the equation of the average concentration  $\bar{c}$  is obtained through:

$$\frac{\partial \bar{C}}{\partial t} + \bar{u}_j \frac{\partial \bar{u}_j \bar{c}}{\partial x_j} = \frac{\partial}{\partial x_j} \left( D \frac{\partial \bar{c}}{\partial x_j} \right) - \frac{\partial}{\partial x_j} \overline{u'_j c'} = 0 \quad (2)$$

In this last equation, the new term  $\frac{\partial}{\partial x_j} \overline{u'_j c'}$  which connects velocity and concentration fluctuations represents an unknown. This term is generally called turbulent flow of concentration or mass this translates the mechanism of turbulent dispersion. In most industrial applications with large Reynolds numbers, the term molecular diffusion will be neglected in the term turbulent dispersion.

Assuming that the average velocity field and the boundary conditions of the fluid domain are known, the calculation of the mean concentration of a passive scalar in a turbulent flow is therefore based on the resolution of the Eq. (2). This equation has four unknowns: the concentration  $c$  and three components of the flow vector  $u'_j c'$ .

The closure of the transport Eq. (2) is more used in CFD codes, this closure directly links the mass fluxes  $u'_j c'$  to the average concentration gradient. This term can be related

to its average gradient by analogy to Flick's law and by introducing the concept of turbulent diffusivity  $D_t$  as it is shown in the following relation:

$$\overline{u'_j c'} = -D_t \frac{\partial c}{\partial x_j} \quad (3)$$

In several calculation codes, the turbulent diffusivity  $D_t$  is estimated as a function of the turbulent viscosity  $\nu_t$  and the number of turbulent Schmidt  $Sc_t$  using the following relation:

$$D_t = \frac{\nu_t}{Sc_t} \quad (4)$$

The turbulent Schmidt number, by default is defined as a constant  $Sc_t = 0.9$  for the CFX code [5] and equal to 0.7 for other codes.

### 3 Brief description of the ROCOM test facility

The ROCOM model is characterized by Real geometry of a KONVOI-type reactor at a linear of 1:5 scale, high similarity of RPV internals, four individually operated loops with flow meters and high quality concentration measurements with wire sensors.

The mesh sensors are placed at four positions in the circuit: RPV inlet nozzle, Upper Downcomer, Lower Downcomer and Core inlet.

The first sensor is connected to the inlet nozzle of the test facility in the loop N°1 and thus records the tracer concentration at the ROCOM inlet. The second and third sensors are respectively located at the entrance and exit of the downcomer. These sensors are constructed as a ring of diameter corresponding to that of the Downcomer (annular space 63 mm). Each sensor forms a measurement matrix of  $16 \times 16$  crossing points. The fourth sensor is integrated with the core support plate to measure tracer concentration at the inlet core. The Fig. 1 summarizes this brief description of the ROCOM facility and for more information regarding this facility see the references [6–8].

As we pointed out previously in Sect. 1 that the measurement of the tracer concentration is based on the measured local conductivities which will then be connected to the standard reference values which correspond to the unaffected primary liquid (demineralised) and the liquid injected into the inlet nozzle of the installation. The result is a passive scalar that instantly characterizes the tracer distribution at any given time or location in the flow field. This scalar is dimensionless and can be calculated as follows:

$$\theta_{x,y,z,t} = \frac{\sigma_{x,y,z,t} - \sigma_0}{\sigma_1 - \sigma_0} = \frac{C_{x,y,z,t} - C_0}{C_1 - C_0} \quad (5)$$

The measured values ( $\sigma_0, \sigma_1$ ) which represent respectively: the initial conductivity of the water in the pilot facility before the opening of the valves and the conductivity of the injected water are transformed into scalar representing the concentration of the mixing in space and time  $\theta(x, y, z, t)$ . More details can be found in [3, 6].

### 4 Grid generation

A hybrid mesh (hexa–tetra) with ICEM CFD was used to mesh the ROCOM geometry which was composed of two parts: Downcomer and lower Plenum, Fig. 2.

This mesh sensitivity study was carried out in partial operating state as shown in Fig. 3. The flow rate supplied by the pump of the cold-leg (CL1) of the primary circuit of the installation is  $185 \text{ m}^3/\text{h}$ , the pumps (2, 3, and 4) are stopped. The flow is steady state.

The mesh sensitivity analysis makes it possible to determine which mesh is the most appropriate, that is to say, from which moment it is no longer necessary to refine the mesh. For this purpose, a study of the steady state flow velocity distribution was carried out on a cross section in the Downcomer Fig. 4, influenced by four meshes (grids) of different sizes. Then, the results were compared to establish the reproducibility status of the code.

Four levels of refinement are tested. For each refinement level, two mesh type are performed, one for the Downcomer (hexa-mesh) and the other for the Lower Plenum (tetra-mesh).

The mesh was refined on the perforated drum, the core support plate and to the cold leg wall regions in each of the mesh; we realize a slight tightening. The grid convergence is mentioned in the Fig. 5. The third mesh M3 was considered for the simulation because; it gives a good ratio between CPU and the precision of calculation.

The final number of elements constituting each part of the geometry is shown in Table 1.

The geometrical characteristics of the internal elements encountered in the lower Plenum have two different functions: to support the reactor core and to homogenize the flow entering the core by breaking up the largest vortices generated by the turbulent flow in order to reduce the vibrations induced on the structures reactor [9].

A wide variety of geometries can be found in the lower layer of nuclear reactors and even in test models. In any case, these details must be taken into account, either with a fine geometric description, or with some simplifications followed by a modeling allowing to correctly including the effects of mixing as well as the resistance to the flow.

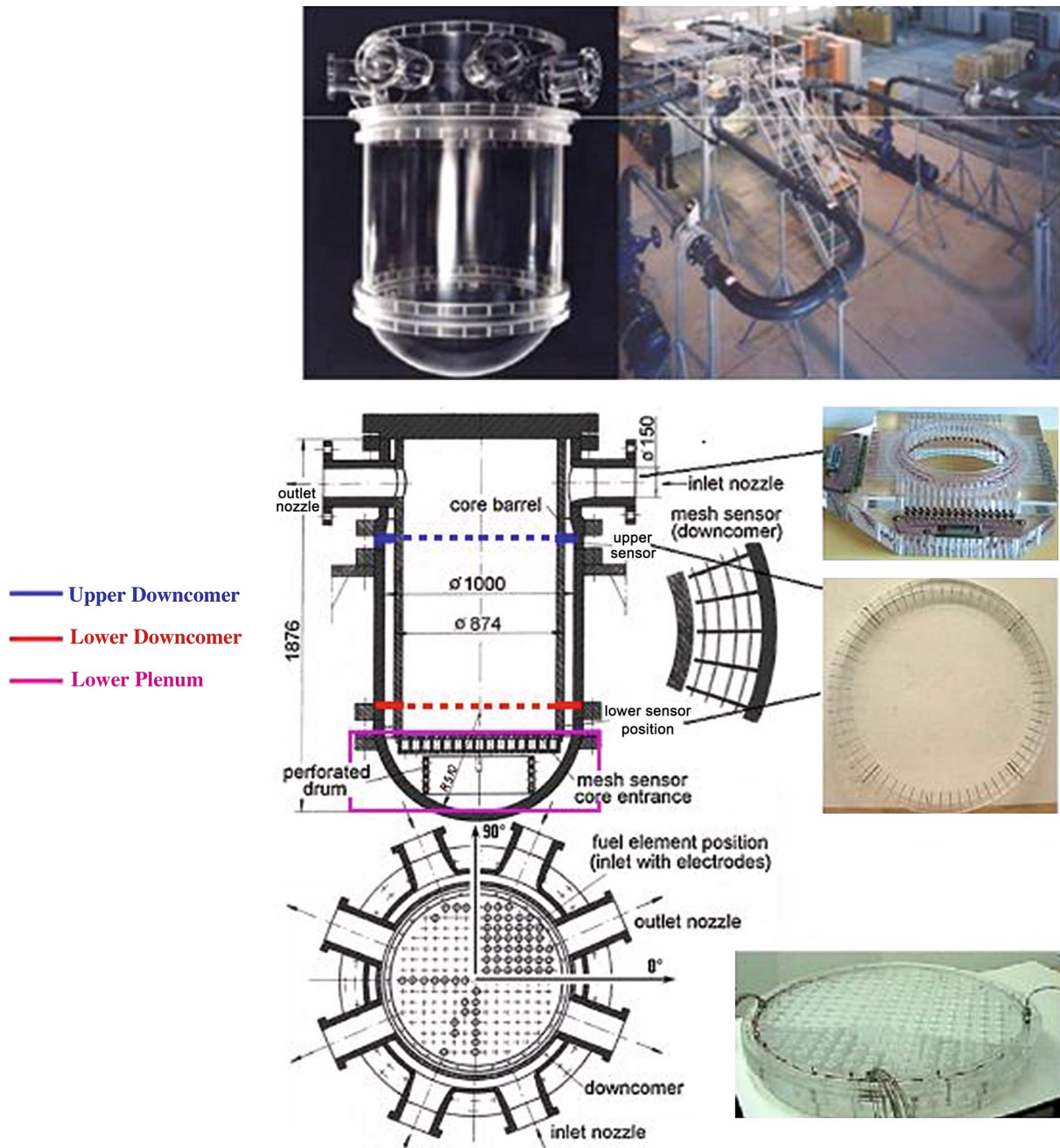


Fig. 1 Rocom test facility [2]

However, a difficulty relative to mesh often encountered in the first case, because a large number of small geometric details must be explicitly meshed (for example, hundreds of support columns, thousands of holes, etc.). This has two main implications is that the mesh gives a very large number of cells, because the maximum size of the cells is imposed locally by geometric scales, which can be very small (of the order of a centimeter or a millimeter), it is almost impossible to generate a good quality hexahedral mesh, so tetrahedral grids are usually the only

feasible option. For this reason geometric simplifications were adopted, compensated by an adequate modeling [9]. This modeling must introduce additional pressure loss in order to properly take into account the flow resistances.

This modeling must introduce an additional pressure drop in order to properly take into account the flow resistances as in the case of this study where the Lower Plenum which has been modeled by a porous zone.

Porous media are modeled by the addition of a momentum source term to the standard fluid flow equations. The

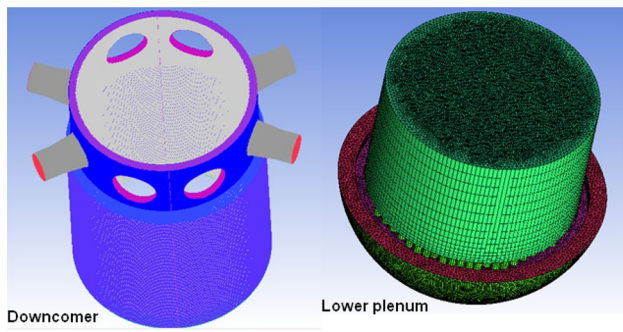


Fig. 2 Mesh generation

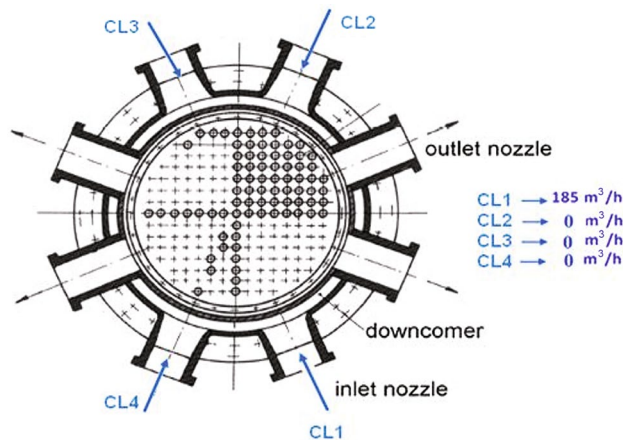


Fig. 3 Partial operating condition studied

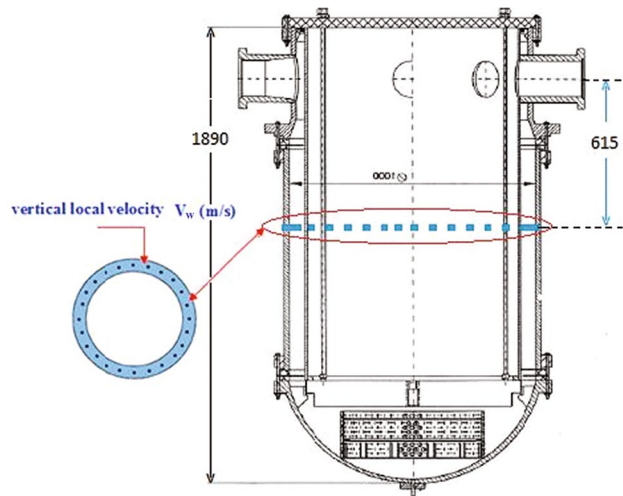


Fig. 4 Vertical local velocity calculation plan  $V_w$  (m/s)

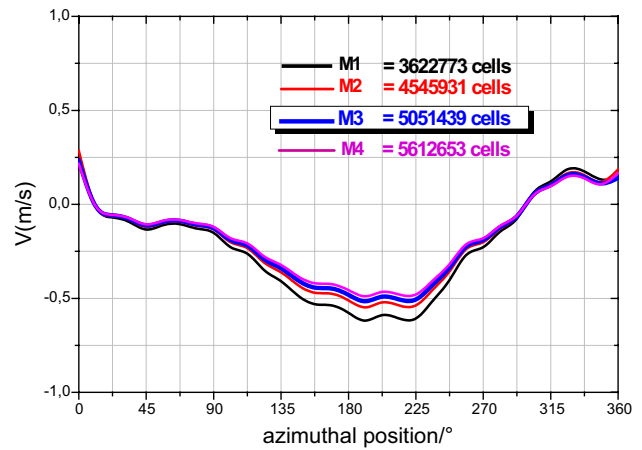


Fig. 5 Grid mesh convergence

Table 1 Grid information

Mesh type	Parts	Number of cells
Hexas	Downcomer	1014841 × 4
Tetra	Lower plenum	992,075
Total number of cells		5,051,439

source term is composed of two parts: a viscous loss term and an inertial loss term.

$$S_i = - \left( \sum_{j=1}^3 D_{ij} \mu V_j + \sum_{j=1}^3 C_{ij} \frac{1}{2} \rho |V_j| C_j \right) \quad (6)$$

The first term of this equation represents the viscous loss and the second represents the inertial loss term.  $S_i$  is the source term for the momentum equation,  $D$  and  $C$  are prescribed matrices. If the porous medium is isotropic,  $S_i$  can be simplified as follows:

$$S_i = \frac{\mu}{\alpha} V_i + C_2 \frac{1}{2} \rho |V_i| V_i \quad (7)$$

$S_i$ : momentum source term (Pa/m);  $\mu$ : dynamic viscosity (Pa.s);  $C_2$ : inertial resistance coefficient (1/m);  $V_i$ : average velocity in the flow direction (m/s);  $\alpha$ : permeability of the medium.

In the present case, the pressure loss are due to a turbulent flow over geometrical discontinuities, and are thus expected to be dominated by the quadratic term, the linear term being thus negligible. The above equation thus reduces to the form below:

$$S_i = C_2 \frac{1}{2} \rho |V_i| V_i \quad (8)$$

Additional pressure loss is applied to the support plate and the perforated drum in the core area of test facility in

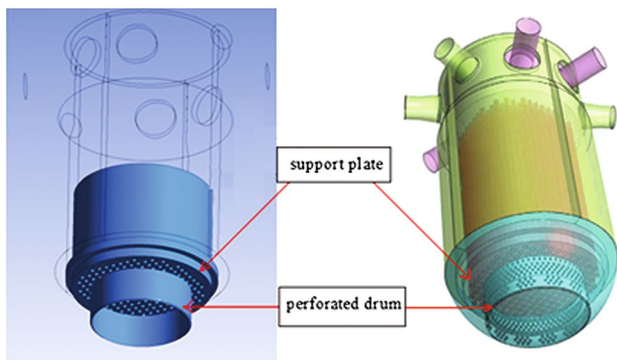


Fig. 6 Modeling of the core area of the ROCOM installation

Table 2 Inertial resistance coefficient  $C_2$  of the modeled zones

Modeled zones	Porosity $\gamma$ [-]	Coefficient of pressure loss	Inertial resistance coefficient $C_2$ [ $m^{-1}$ ]
Core support plate	0.229	10.5	85
Perforated drum	0.208	13.1	13

order to compensate for the assumptions of the simplifications formulated during the modeling. In this study, the elements modeled by a porous medium are the core support plate and the perforated drum shown in Fig. 6.

Different models of additional pressure loss are available in the Ansys CFX code with other types of correlations [5], requiring to calculate the closing coefficients according to the geometric configuration. The Idle'cik manual [10], can provide useful indications in many cases, but in other cases the experimental data are necessary [11]. The directional loss model is the most suitable for our case, because it allows to define different flow resistance in different directions.

The directional loss model is best suited to our case because it allows different flow resistances to be defined in different directions. This model takes the form of Eq. (7) "Darcy–Forchheimer".

The pressure loss coefficients are necessary to estimate the pressure loss created by the modeled regions (core support plate and perforated drum) of the ROCOM installation. These coefficients are determined experimentally using the characteristics of the porous medium such as

porosity. The pressure drop coefficient allows us to determine the inertia resistance coefficients ( $C_2$ ) of the porous medium in the direction of flow of each modeled element. (Table 2).

### 5 Experimental test ROCO M-12

The ROCOM-12 test, is a benchmark designed by the ROCOM test facility as part of the IAEA's Coordinated Research Project (CRP), represents a transient event generated by a single pump start in the primary circuit of the installation and the other three pumps are stopped with a return to the branches connected to the stop state of the pumps. The ROCOM-12 plug mixing experiment was performed by simulating the volume of deborated water plugs for more details see [7]. The boundary conditions of ROCOM-12 are presented in Table 3. This test brought on the problem of boron dilution, in which a non-borated volume slug water is injected into one of the cold legs and the another three legs remaining stagnant Fig. 7, and the tracer concentration that was used in the test is measured at the Upper Downcomer, Lower Downcomer and at the core inlet of the test facility to assess the degree of heterogeneity when starting the pump and at the same time to test the predictive ability of the used CFD code [12].

### 6 Computational modeling

The simulations performed according to the specifications of the ROCOM mixing experiment, using the CFX12 code, are carried out at a variable mass flow rate through the CL1 loop which corresponds to 2.91 m/s inlet velocity after 30 s and a low flow return (beak flow) for the other three inlet nozzles, the tracer being injected for a short period in the unsteady flow field through the inlet nozzle CL1. A passive scalar was used to describe the mixing process. The outlet boundary conditions were pressure controlled. The defined scalar assumes values between 0 and 1. The value 0 corresponds to the absence of tracer, while the value 1 represents the maximal concentration of the normalized tracer of the cooling fluid from loop 1. In this work, a simulation of turbulent flow and mixing in ROCOM facility were carried out by solving the Reynolds Averaged Navier–Stokes (RANS) equations with SST turbulence

Table 3 ROCOM-12 slug mixing experiments

Run	Ramp length [s]	Final volume flow rate [m3/h]	Slug volume [m3]	Initial slug position [m]	Status of unaffected loops	Single realisa-tions
ROCOM-12	14	185	8	10	Open	5

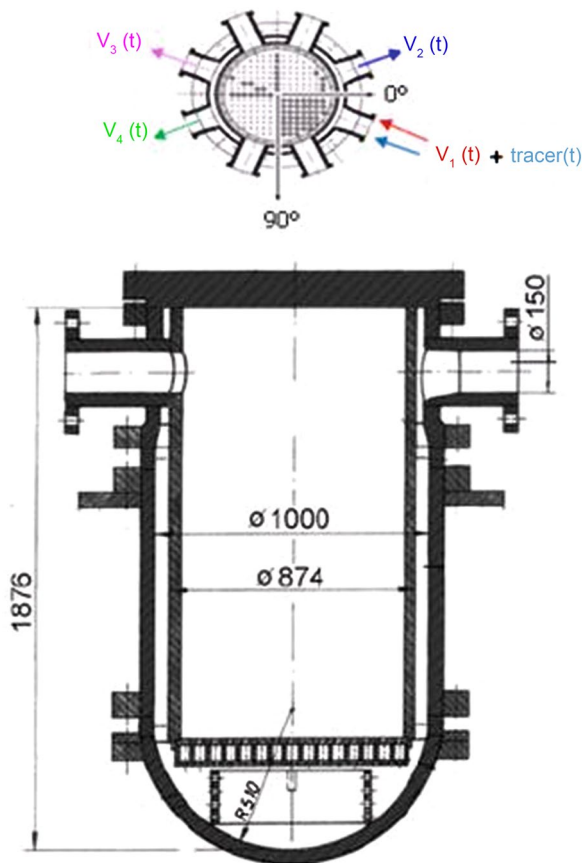


Fig. 7 Locations of inlet boundary conditions of ROCOM-12 test

model combined to a transport equation of an additional, user-defined, scalar variable (mixing scalar (MS) simulating the tracer. The turbulence model (SST) was used in this work for several reasons. This model combines the robustness and accuracy of the  $k-\omega$  model in the near-wall region and the efficiency of the  $(k-\epsilon)$  model away from the wall. In addition, it has been shown, from the literature search, that this model is relevant for a large class of flows because it can properly capture near-wall recirculation [13].

Many previous works similar to our work, based on this model show its adequacy and relevance [8, 14–16].

The numerical simulation was carried out with the following assumptions [12]:

- Transient solver;
- Incompressible fluid: water;
- Coolant temperature: 25 °C;
- Pressure: 1 bar;
- Density: 997 kg/m<sup>3</sup>;
- Dynamic viscosity: 8.899 e-4 kg/m s;
- Variable velocity: inlet boundary conditions;
- Pressure controlled: outlet boundary condition;
- Turbulent intensity: 5%.

In this study, the “High Resolution” scheme was used with a second order Backward Euler temporal discretization scheme, the “High Resolution” scheme was adopted for this study since it makes it possible to obtain the value of the most appropriate coefficient ( $\beta$ ) for the advection scheme and a implicit scheme was used to approximate the transient terms.

## 7 Initial and boundary conditions

The calculations are performed on eight parallel processors (CPU 2.66 GHz each) containing 16 GB RAM. The simulated time period is 30 s. The time step used is  $\Delta t = 0.05$  s.

### 7.1 Boundary conditions relating to velocities entry

The input velocities of each cold leg of the test facility are formulated identically to the experimental conditions.

The inlet velocity of the active loop N°1,  $v_1(t)$  is given experimentally and recorded every 0.1 s over a time interval of 30 s. For the other passive loops, the shut-off valves are open. Therefore, an inverse flow is established in these loops. The maximum value of this reverse flow corresponds to about 5% of the nominal value in each of the loops Fig. 8.

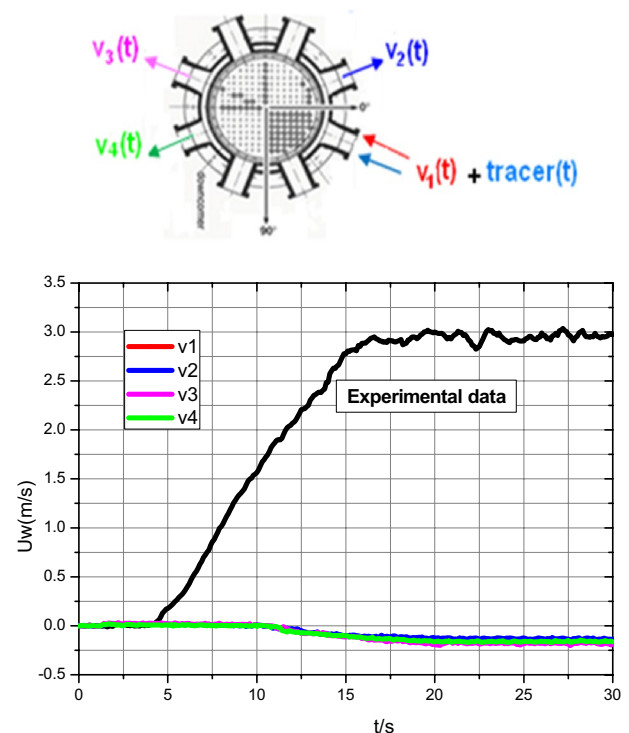


Fig. 8 Velocity inlet

## 7.2 Boundary conditions relating to tracer

The tracer was injected through the Inlet nozzle N°1. Experimental tracer data was introduced through expressive language specific to Ansys CFX CEL (CFX Expression Language) code. The tracer was carried out as an additional variable. This is introduced into the transport equation in the CFX-Pre as a passive scalar. Figure 9 shows the experimental values of the tracer injected at the Inlet nozzle N°1 during the experimental test.

## 8 Results and discussion

The salt solution injected (tracer) through the cold leg N°1 of ROCOM test facility, mixes with demineralized water already contained in the test facility by the effect of turbulence flow. The mixing turbulent thus affects the spatio-temporal distribution of the tracer. The tracer concentration can be expressed in terms of the mixing scalar and this parameter will be used in the following to compare the numerical results with the experimental data. All the figures in this section show the time and space distribution of tracer concentration at the inlet cold leg, upper Downcomer, lower Downcomer, and at the core inlet of ROCOM test facility Fig. 10. The discussion of the results obtained mainly involves a qualitative analysis aimed at verifying that the solution obtained is physically possible and realistic.

### 8.1 Tracer concentrations and velocities at inlet nozzles

The same experimental results at the input of the computational domain are obtained identically by the Ansys CFX code after the start of the computation. The velocity

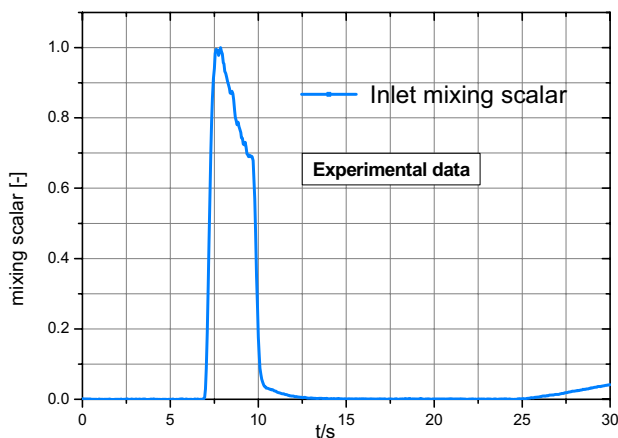


Fig. 9 Tracer inlet

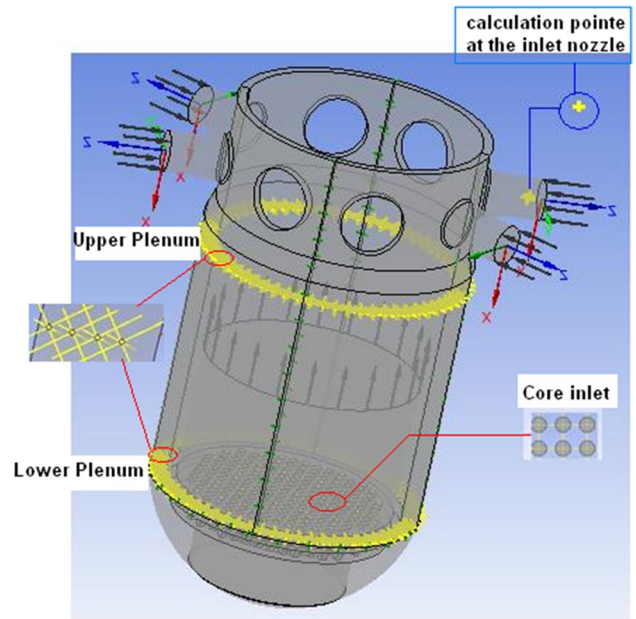


Fig. 10 The places of calculation and comparison of results

distribution at the inlet of the four nozzles is illustrated in Fig. 11, while Fig. 12 shows the tracer distribution at point-1 of the inlet nozzle N1.

### 8.2 Tracer concentrations at Upper Downcomer in terms of time

Figures 13 and 14 have shown respectively the tracer average and maximum distribution which indicates the variation of the mixing scalar over a 30-s time interval at the Upper-Downcomer. These results counted in this place are relatively in good agreement in term of time with

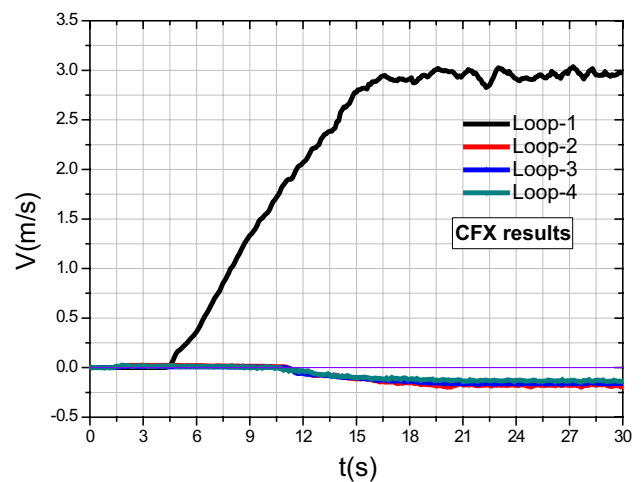


Fig. 11 Velocities distribution at the four inlet nozzles



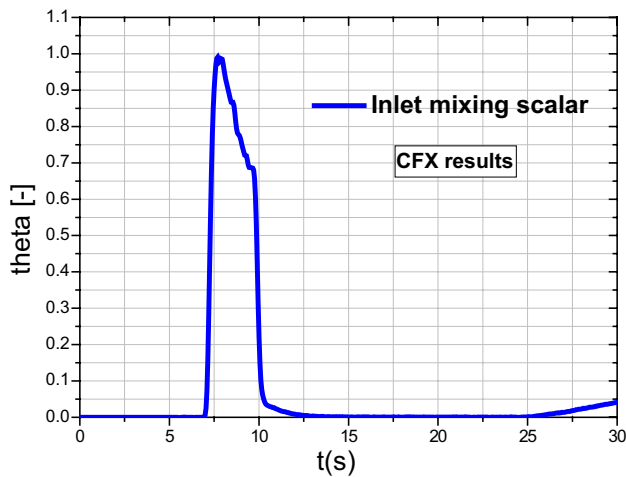


Fig. 12 Inlet mixing scalar at point-1 in inlet nozzle N°1

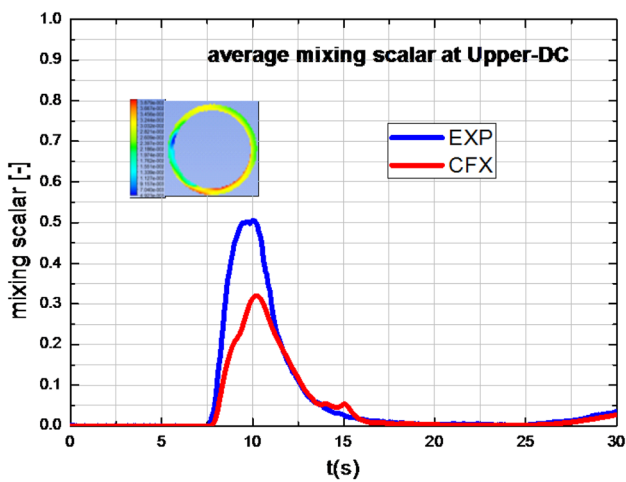


Fig. 13 Time dependent averaged mixing scalar at Upper-Downcomer

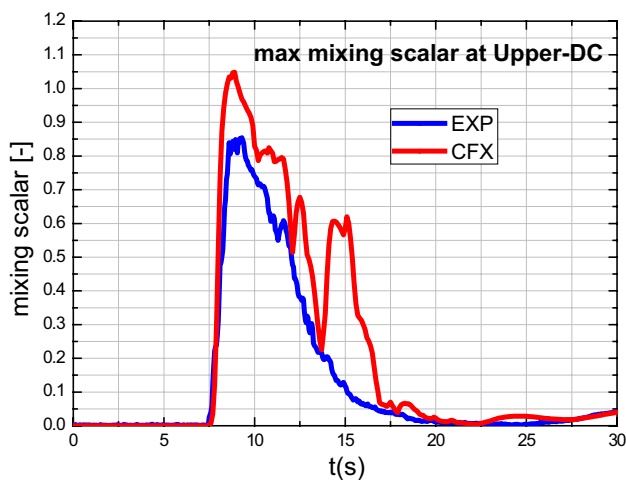


Fig. 14 Time dependent Max mixing scalar at Upper-Downcomer

the experimental data. Figure 14 also shows oscillations (peaks) in the distribution of the concentration between the moment 9 and 17 s.

### 8.3 Tracer concentrations at Upper Downcomer in terms of space

Figure 15 shows the measured and calculated tracer distribution in Upper-Downcomer after 10 s. Noted that the tracer concentration values are very low in the azimuthal zone between (135° and 270°), while maximum values are recorded outside this zone, this zone is far from the tracer injection point. A good concordance was found between the results of calculations and those of the experimental.

The opposite of the previous case was observed for the results recorded at the instant 15 s; in Fig. 16. It has been found that the tracer values in the azimuthal zone (135° and 250°) are high relative to the concentration values outside this zone, this amount to the decrease in tracer concentration or dilution of the tracer from this time of 15 s. The results obtained by the code with those of the experimental are qualitatively in agreement.

The next two figures show the temporal distribution of tracer concentration at a fixed azimuthal position in Upper-Downcomer. The two azimuthal positions 8° and 30° give the same concentration profile at the same time interval with maximum concentrations between 8 and 12 s, which indicate that the two maxima of both Figs. 17 and 18 reside in a recirculation zone in the annular space below the inlet nozzle. The experimental and computer results are in good agreement, however, a slight difference between the maximum values of the two results appeared between 8 and 12 s under the inlet nozzle, which can be explained by the physical or numerical models adapted for

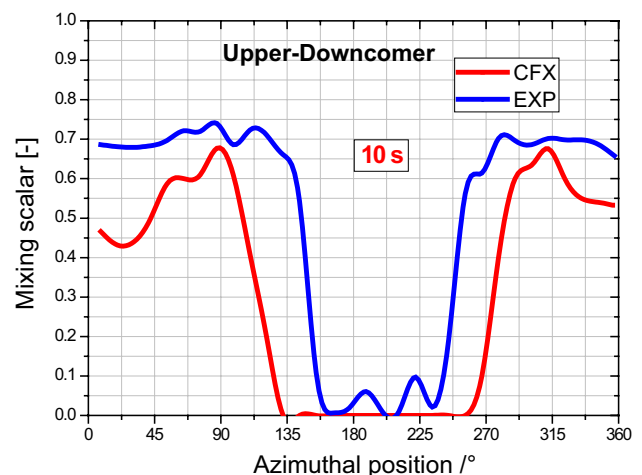


Fig. 15 Azimuthal distribution of tracer at Upper-DC in the moment 10 s

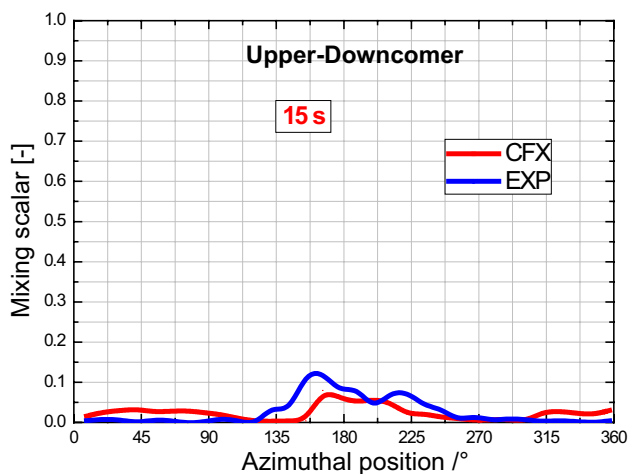


Fig. 16 Azimuthal distribution of tracer at Upper-DC in the moment 15 s

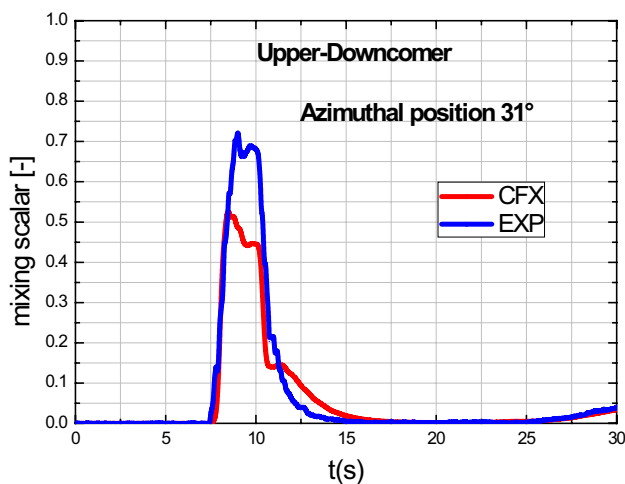


Fig. 18 Temporal distribution of tracer at Upper-DC in the Azimuthal position 31°

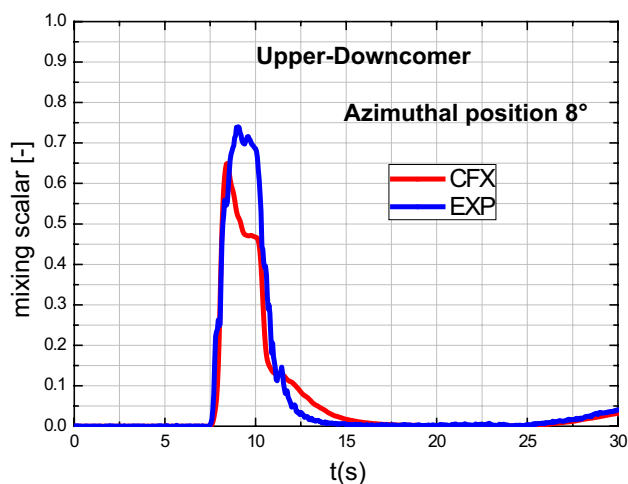


Fig. 17 Temporal distribution of tracer at Upper-DC in the Azimuthal position 8°

this calculation cannot predict the parameters of a recirculation zone.

### 8.4 Tracer concentrations at Lower Downcomer

This section examines the average and maximum temporal distribution of tracer in Lower-Downcomer. For the average profile of the concentration illustrated in Fig. 19, noted a good agreement between the results obtained by the code and that of the experimental. Nevertheless, the two profiles are separated a little from each other between 10 and 15 s and this always due to the recirculation zone located under the inlet nozzle.

For the case of the profile representing the maximum distribution of tracer concentration on the

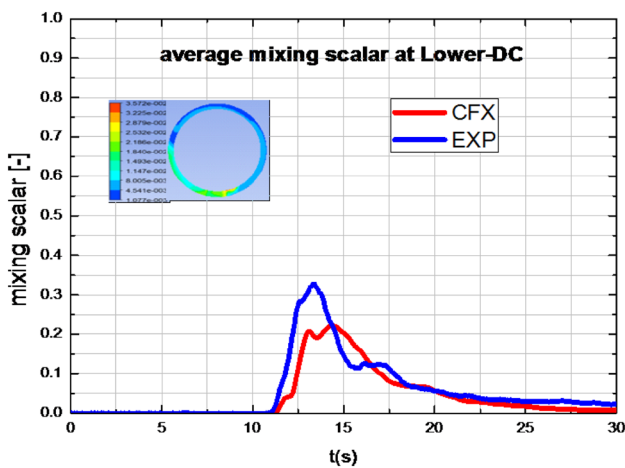
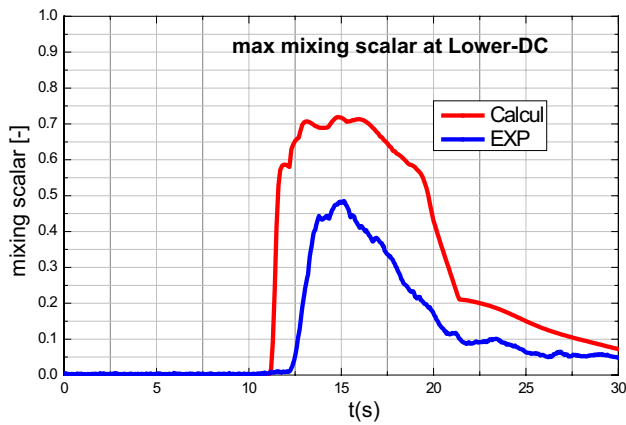


Fig. 19 Time dependent global averaged mixing scalar at Lower-Downcomer

Lower-Downcomer, Fig. 20, and the difference between the two results (calculation-experimental) were observed is greater compared to the case of the average profile.

### 8.5 Tracer concentrations at the core inlet

In this last part concerning the results, we treat the average and local temporal distribution of the tracer concentration at the core inlet. The average time distribution of the tracer at the core inlet obtained by the code is in agreement with the experimental data Fig. 21, but the exception which makes the difference between the experimental results and the computation is always appearing at an interval of the time equal nearly 7 s located in the middle of the interval of the global time.



**Fig. 20** Time dependent global Max mixing scalar at Lower-Downcomer

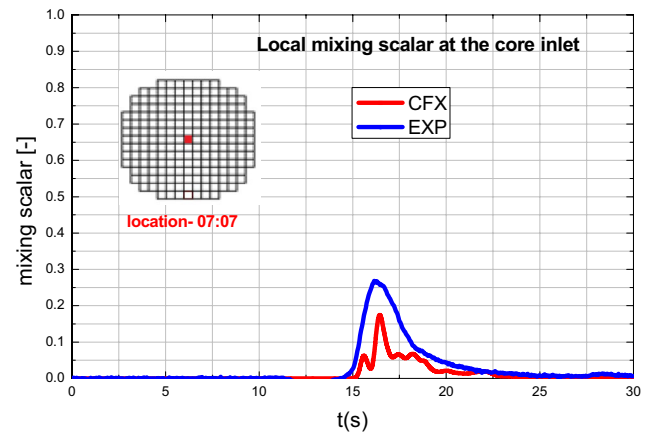


**Fig. 22** Time dependent local mixing scalar at the core inlet location (07:07)

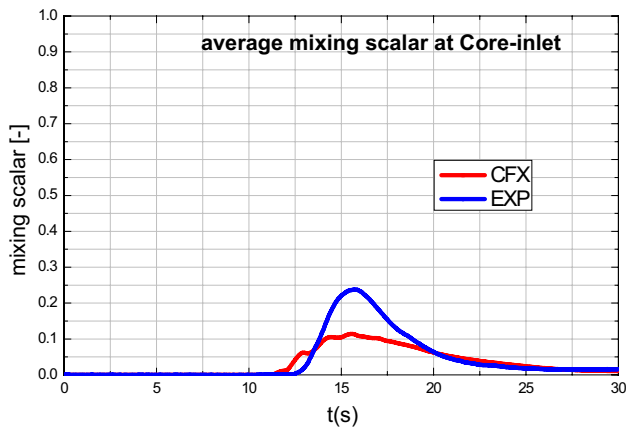


**Fig. 21** Time dependent global average mixing scalar at core-inlet

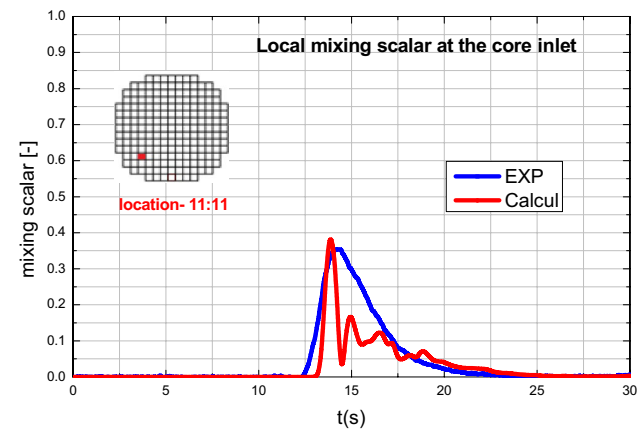


**Fig. 23** Time dependent local mixing scalar at the core inlet location (11:11)

The same remarks as those observed on the average distribution can be applied to the case of the local distribution of the tracer at the core inlet, Figs. 22 and 23. These figures show the time dependent local mixing scalar at the core inlet position in the middle and near the wall. The results are in good agreement with the experimental data outside the time interval mentioned above. It is generally noted that the measured concentration is always higher than that calculated in terms of average values and the inverse in terms of the maximum values. Note that the results of calculation and those of the experimental are a little discarded from each other in a range of 5–7 s in the middle of the time interval. But qualitatively there is a good agreement between both results.

## 9 Conclusion

The present study is part of the IAEA's CRP framework, and deals with a reference problem of boron dilution used to study safety issues related to PWRs currently in service, as well as new concepts. They focus on the mechanisms related to the mixing phenomenon relative to the boron dilution and focuses more particularly on the experimental study of a tracer injection performed on the ROCOM test facility. The numerical results were compared with available experimental benchmark data, which consist of tracer concentration measurements at several locations such as the core inlet, the upper and lower Downcomer. From a qualitative point of view, the spatial and temporal distributions of tracer concentration in Downcomer and at the core inlet are reasonably predicted by the Ansys CFX code.

**Acknowledgements** The first author expresses his thanks to the Birine Nuclear Research Center for the provision of computer equipment and the Ansys CFX code license. This document contains experimental data that were produced in the Experimental ROCOM facility at Helmholtz Zentrum Dresden-Rossendorf. The authors of this article are grateful to the team of the ROCOM test facility and wish to thank.

## Compliance with ethical standards

**Conflict of interest** All authors have no conflict of interest to declare.

## References

- Spalart PR, Venkatakrisnan V (2016) On the role and challenges of CFD in the aerospace industry. *Aeronaut J* 120(1223):209–232. <https://doi.org/10.1017/aer.2015.10>
- Prasser HM, Grunwald G, Höhne T, Kliem S, Rhode U, Weiss FP (2003) Coolant mixing in a pressurised water reactor: deboration transients, steam-line breaks, and emergency core cooling injection. *Nucl Technol* 143:37–56. <https://doi.org/10.13182/NT03-A3396>
- Höhne T, Kliem S, Ulrich B (2006) Modeling of a buoyancy driven flow experiment at the ROCOM test facility using the CFD codes CFX-5 and Trio U. *Nucl Eng Des* 236:1309–1325. <https://doi.org/10.13182/NT03-A3396>
- Mydlarski L, Warhaft Z (1998) Passive scalar statistics in high Péclet-number grid turbulence. *J Fluid Mech* 358:135–175. <https://doi.org/10.1017/S0022112097008161>
- ANSYS CFX-Solver Theory Guide (2013) Release 14.5. ANSYS Inc., Canonsburg
- Höhne T, Kliem S, Prasser HM, Rohde U (2003) Experimental and numerical studies inside a reactor pressure vessel. In: 4th ASME/JSME joint fluids engineering conference, Hawaii, USA. <https://doi.org/10.1115/FEDSM2003-45294>
- Hewitt G, Vassilicos C (2005) Prediction of turbulent flows. Cambridge University Press, Cambridge. <https://doi.org/10.1017/CBO9780511543227>
- Kliem S, Sühnel T, Rohde U, Hohne T, Prasser HM, Weiss FP (2008) Experiments at the mixing test facility ROCOM for benchmarking of CFD codes. *Nucl Eng Des* 238:566–576. <https://doi.org/10.1016/j.nucengdes.2007.02.053>
- Moretti F (2009) Contribution to the assessment of CFD codes for in vessel flow investigation. Dissertation, University of Pisa
- Idel'cik IE (1986) Mémento des pertes de charge: coefficients de pertes de charge singulières et de pertes de charge par frottement. Eyrolles, Paris
- Ahmed SE, Aly AM, Raizah ZAS (2019) Heat transfer enhancement from an inclined plate through a heat generating and variable porosity porous medium using nanofluids due to solar radiation. *SN Appl Sci* 1:661. <https://doi.org/10.1007/s42452-019-0682-2>
- Boumaza M, Moretti F, Dizene R (2014) Numerical simulation of flow and mixing in ROCOM facility using uniform and non-uniform inlet flow velocity profiles. *Nucl Eng Des* 280:362–371. <https://doi.org/10.1016/j.nucengdes.2014.10.018>
- Lee HC, Wahab AKA (2019) Performance of different turbulence models in predicting flow kinematics around an open offshore intake. *SN Appl Sci* 1:1266. <https://doi.org/10.1007/s42452-019-1320-8>
- Kiss B, Boros I, Aszódi A (2008) Recent results of three-dimensional CFD simulations of coolant mixing in VVER-440/213 reactor pressure vessel. In: 18th symposium of AER on VVER reactor physics and reactor safety, Eger, Hungary
- Rohde U, Höhne T, Kliem S, Hemström B, Scheuerer M, Toppila T, Aszodi A, Boros I, Farkas I, Mühlbauer P (2007) Fluid mixing and flow distribution in a primary circuit of a nuclear pressurized water reactor validation of CFD codes. *Nucl Eng Des* 237:1639–1655. <https://doi.org/10.1016/j.nucengdes.2007.03.015>
- Bezrukov YA, Dragunov YG, Logvinov SA, Ul'yanovskii VN (2004) Investigation of the mixing of coolant flows in a VVER vessel. *At Energy* 96(6):432–440. <https://doi.org/10.1023/B:ATEN.0000041205.60891.10>

**Publisher's Note** Springer Nature remains neutral with regard to jurisdictional claims in published maps and institutional affiliations.